Exogenous Administration of Substance P Enhances Wound Healing in a Novel Skin-Injury Model

ANGEL V. DELGADO,* ALBERT T. MCMANUS,† AND JAMES P. CHAMBERS‡,[1]

Combat Casualty Care Branch and †Research Division, U.S. Army Institute of Surgical Research, Fort Sam Houston, Texas 78234; and ‡Department of Biology, University of Texas at San Antonio, San Antonio, Texas 78249

Soft tissue injury accounts for approximately 44% of all wounds in both the military and civilian populations. Following injury to soft tissue, Substance P (SP) and other neuropeptides are released by cutaneous neurons and modulate the function of immunocompetent and inflammatory cells, as well as epithelial and endothelial cells. The interaction between these components of the nervous system and multiple target cells affecting cutaneous repair is of increasing interest. In this report, we describe the effects of SP on wound repair in a novel, laser-induced, skin-wound model. Gross and histologic examination of laser-induced injury revealed that exogenously administered SP affects wound healing *via* neurite outgrowth, in addition to adhesion molecule and neurokinin-1 receptor involvement *in vivo*. All SP effects were decreased by pretreatment with Spantide II, an SP antagonist. The elucidation of SP-mediating mechanisms is crucial to firmly establishing the involvement and interaction of the peripheral nervous system and the immune system in cutaneous repair. Findings presented here suggest that SP participates in the complex network of mediators involved in cutaneous inflammation and wound healing. Exp Biol Med 230:271–280, 2005

Key words: Substance P; CO_2 laser; wound healing; neurite outgrowth

Our understanding of Substance P (SP) has evolved considerably since it was first discovered in 1931. Seventy plus years of research have led to our current understanding of the diverse functions of this neuropeptide. Considerable evidence suggests that neurogenic stimuli affect cellular events involved in inflammation, cell proliferation, and the extracellular matrix, as well as induce cytokine and growth-factor synthesis (1). Neuronal and immune cells both produce SP. Published reports show that morphine upregulates the production of SP produced by human monocytes and lymphocytes in culture (2). Lai *et al.* (3) demonstrated SP mRNA synthesis in human white blood cells. It has been demonstrated that loss of sensory innervation impairs wound healing in rats (4). Furthermore, it has been shown that, compared to uninfected subjects, immunocompromised, HIV-infected individuals have elevated plasma SP levels (5).

Axons containing SP are primarily found in connective tissue surrounding vessels and at the border between adventitia and media (muscle layer), but they are also present in the dermis and epidermis (6–8). There is strong evidence that injured nerve endings release SP in support of the neurogenic mediation of inflammation and vasodilatation in early wound repair. Through activation of the release of histamine from dermal mast cells in human skin, SP indirectly evokes vasodilation (9). These effects are not restricted to the initial point of stimulus, but are also observed in the surrounding area. This indicates that nerve impulses, in addition to traveling centrally, also move collaterally *via* branches that pass antidromically to unstimulated nerve endings, which results in the release of neuropeptides (axon reflex; Ref. 10).

Nerve fibers that produce SP are absent in the epidermis and extracellular matrix in early burn wounds, but repopulate the wound bed following neovascularization, originating in the deep reticular dermis and wound edge (11). Healing of injured tissue requires adequate organizational and functional reactions of the primary afferent sensory nerves and the microcirculatory system. Sensory neuropathies are associated with insufficient coordination of these processes predisposing trophic disorders of the skin to ulceration (12) and connective tissue malfunction (13). Neovascularization of the vascular rabbit cornea is induced by SP (14), which is also known to cause neurite outgrowth

This research was funded in part by the U.S. Army Medical Research and Materiel Command and the National Institutes of Health Grant GM08194. The opinions or assertions expressed herein are the private views of the authors and are not to be construed as official or as reflecting the views of the U.S. Department of the Army or the U.S. Department of Defense.

[1] To whom correspondence should be addressed at Department of Biology, University of Texas at San Antonio, San Antonio, TX 78249. E-mail: jchamber@utsa.edu

Received September 10, 2004.
Accepted January 23, 2005.

1535-3702/05/2304-0271$15.00

in the dorsal-root ganglia of embryonic chicks (15). Furthermore, *in vivo* experiments have shown SP to stimulate angiogenesis (14, 16, 17), which supports the hypothesis that tissue and nervous-system interactions promote healing. Potent proliferative effects on cultured fibroblasts are exerted by SP (14, 18, 19), which has also been shown to act through neurokinin (NK) receptors to stimulate proliferation of cultured keratinocytes (20, 21). The primary interaction of SP is with the NK-1 receptor, but it also interacts with lower affinity with NK-2 and NK-3 receptors. Additionally, neuropeptides have been shown to be both stimulatory and inhibitory to the proliferation of keratinocytes (22). These data suggest that neuropeptides released from peripheral nerve endings in association with tissue injury not only affect vasodilation associated with the inflammatory response, but may also stimulate proliferation of epithelial, vascular, and connective tissue cells.

Materials and Methods

Adult male Sprague-Dawley rats (350–400 g) were used throughout this study. Animals were housed in standard polycarbonate cages with free access to rodent chow and water and were maintained on a 12:12-hr light:dark cycle in a climatically controlled room. All animals used in this study were maintained in a facility accredited by the Association for the Assessment and Accreditation of Laboratory Animal Care International. Additionally, this study was approved and sanctioned by the Institutional Animal Care and Use Committee of the U.S. Army Institute of Surgical Research, Fort Sam Houston, Texas. All animals received humane care in accordance with the National Institutes of Health's *Guide for the Care and Use of Laboratory Animals.*

Rat Hair Growth-Cycle Synchronization. Rats possess patches of skin in the telogen phase, in juxtaposition to skin in the anagen phase, in patterns that vary among rats. Hair follicles are at rest in the telogen phase, when the skin is thinner and less vascular than that observed for the anagen phase. For laser ablation to occur at consistent depths with respect to anatomical landmarks following the application of a given amount of energy, the site to be lesioned must be in the anagen phase. The anagen phase was achieved according to the method of Zawacki and Jones (23). Thirteen days before laser treatment, hair on the back of the anesthetized animal was clipped just wide of the intended laser-wound site using animal clippers (#40 blade). The back of the animal was then treated with Magic Shave Red (Carson Products Co., Savannah, GA), a barium sulfide depilatory cream, to stimulate telogen-phase sites to the anagen phase, bringing the skin to a uniform thickness. Cream was removed after 5 mins. Animals were placed back into their respective cages and allowed to recover until the date of treatment synchronizing the hair-follicle cycle.

CO_2 Laser Deep-Skin Wound Rat Model. The laser used for this study was a 150XJ CO_2 surgical laser system equipped with a model 797XJ x, y-galvanized computerized scanner and a 200-mm hand piece. The CO_2 laser emits in the far-infrared range at a wavelength of 10.6 μm. Because of this particular wavelength, the CO_2 laser has a very high coefficient of absorption for water. Because soft tissue is normally 70%– 90% water, water is used as the standard for biologic tissue and is often a good model for nonpigmented soft tissue. Thirteen days post–barium sulfide treatment, animals were anesthetized using an inhalation anesthetic (i.e., isoflurane gas). Barium sulfide depilatory cream was applied as previously described. Before injury, the analgesic ketoprofen (5 mg/kg im) was administered to all animals across all groups, control animals included. The elimination half-life for ketoprofen is 2.1 hrs; thus, the drug is effectively eliminated at 15 hrs postadministration. The use of ketoprofen as described above was required by the Institutional Animal Care and Use Committee of the U.S. Army Institute of Surgical Research. Additionally, the antibiotic Baytril (Bayer Corp., Shawnee Mission, KS) was administered preoperatively to all animals as a single dose of 2.5 mg/kg to ensure that there were no complications arising from infection following laser injury.

A laser injury was administered with various energy intensities. All laser safety precautions were adhered to as designated in U.S. Army Institute of Surgical Research guidelines. Animals were kept warm and monitored until fully awake. All animals were housed in the animal intensive-care chamber until fully recovered. At the end of the recovery period, animals were returned to their holding room for regular monitoring. Room temperature was kept at 78°F–82°F, and humidity was kept at approximately 50%. Food and water were allowed *ad libitum* for the remainder of the study. At the end of examination period, animals were euthanatized and full-thickness skin samples were collected and fixed for routine histology (i.e., hematoxylin eosin, Mason's Trichrome Stain) and immunohistochemistry (i.e., NF-200, NK-1, $\alpha_5\beta_1$ integrin).

Wound-Depth Measurements. The wound-depth measurements were made using 4× magnification images of entire cross-sectional planes of skin using the integrated imaging and calibration system, MetaMorph (Nikon, Lewisville, TX). Measurements were standardized by measuring from the top edge of the panniculus carnosus layer to the point of evident collagen involvement in the affected area.

Wound-Healing Scoring. Wound-healing scores were determined following both gross and histologic criteria by a board-certified pathologist blinded to the respective treatments. Animals were randomized and assigned an identification accession number corresponding to each specific animal, the identifying key of which was unknown to the scoring pathologist. Points were awarded for necrotic epidermis, necrotic dermis, necrotic hypodermis, edema, lack of granulation tissue, leukocyte infiltrate, absence of new collagen fibers, presence of scab, necrotic adnexa, and absence of epithelization under the scab. Healing scores

were expressed on a scale of 0 to 10, with higher scores indicating poorer wound healing.

Treatment Administration. Exogenous administration of SP (Sigma Chemical Co., St. Louis, MO), Spantide II (SII; American Peptide Co., Sunnyvale, CA), and vehicle (saline) was given in final volume of 200 μl *via* sc injection using a 26-gauge needle. Deposition of SP into the wound was accomplished by injection, entering the sc space from the rostral side of the wound edge until the tip of the needle was at the center of the injury site. Animals remained immobile under anesthesia for 30 mins to allow for maximal dispersion of the injection material.

Tissue Harvesting. Skin tissue samples (2 × 2-cm pieces) were collected while the animal was fully anesthetized at 0, 3, 7, 14, and 21 days postinjury. The skin was excised down to the subpanicular space, ensuring collection of all skin layers as well as the panniculus adiposus and panniculus carnosus layers of the hypodermis. After tissue harvesting, animals were euthanatized by Nembutal (Vortech Pharmaceuticals, Dearborn, MI) overdose.

Immunohistochemical Staining. Tissue samples were collected and immediately fixed in 2% paraformaldehyde/lysine/periodate fixative for 24 hrs. Samples were then washed in phosphate-buffered saline (PBS), placed in Jung tissue-freezing medium (Leica Instruments, Nussloch, Germany), and stored at −80°C. Frozen specimens were trimmed of excess cryoprotectant and mounted onto a Leica cryostat (Leica Instruments). Frozen sections were cut (50 μm) and immediately placed in a 96-well microtiter plate containing PBS. Samples were submerged and not allowed to float or dry out. The staining procedure was performed according to the method of McCarthy *et al.* (24). For staining neurites, a rabbit anti–NF-200 antibody (Sigma Chemical) was used. Detection of SP receptors was accomplished using a rabbit anti–NK-1 antibody (Sigma Chemical).

Detection of intercellular adhesion molecule-1 (ICAM-1) was performed as follows: heparinized, rat whole blood was incubated for 4 hrs with saline (control) or 10^{-7} *M* SP (treatment) *in vitro*. Subsequently, staining of cells was carried out using an anti-rat, ICAM-1, monoclonal antibody labeled with a fluorescent tag. Briefly, 100 μl sodium-heparinized rat blood was incubated with 20 μl 1×10^{-7} *M* SP. Each control contained a 20-μl vehicle. All samples were loosely capped, mixed gently, and incubated at 37°C with 5% CO_2 for 4 hrs. To 100-μl treated blood, 20 μl of anti-rat, ICAM-1, monoclonal antibody (BD PharMingen, San Jose, CA) were added, mixed, and incubated at room temperature in the dark for 15 mins. Excess, unbound antibody was washed by the addition of 2 ml PBS/bovine serum albumin and centrifuged at 200 *g* for 5 mins. Supernatant was carefully decanted and discarded. To the cell pellet material, 2 ml 1X FACS Lysing solution (BD PharMingen) were added, gently vortexed, and incubated at room temperature in the dark for 10 mins. Cells were pelleted by centrifugation at 200 *g* for 5 mins, carefully decanting the supernatant. Cell-pellet material was washed as previously described, resuspended in 400 μl 1% (v/v) formaldehyde, and stored in the dark at 4°C until flow-cytometric analysis. Flow cytometry was carried out using a Becton Dickinson FACSCalibur flow cytometer (BD Bioscience, San Jose, CA) equipped with CellQuest Pro software for data analysis.

Integrins ($\alpha_5\beta_1$) were monitored using an antibody (BD Biosciences, San Jose, CA) and stained with detecting goat antirabbit, fluorescent tag–labeled secondary antibody (Caltag Laboratories, Burlingame, CA). Acquisition of images from stained samples was achieved using an Axiovert 135 inverted microscope (Zeiss, Thornwood, NY) equipped with a CARV fluorescent confocal module (Atto Bioscience, Rockville, MD) and a Quantix CCD camera (Photometrix, Tucson, AZ). Images were acquired using CARVer version 1.2 software (Atto Bioscience).

Histomorphometric Measurements. Quantitative assessment of axonal growth was analyzed by measurement of total length of fluorescent axon and the total mean fluorescence intensity of each sample. Both NK-1 and integrin staining were measured as the total mean fluorescence intensity for each sample. All fluorescence measurements were performed using MetaMorph software integrated imaging system (Universal Imaging Corp., Philadelphia, PA).

Immunohistochemical Quantitative Analysis. Neurite length was quantified by fluorescent confocal microscopy. Tissue slices (50 μm) stained for neurites were confocally imaged, taking 25 images, one every 2 μm. Using Metamorph software, all 25 images were compressed into a single, two-dimensional image. A background subtraction was performed from the compressed image and then binarized to generate a black-and-white image from a gray-scale image. The image was dilated to analyze the pixel composition, and a pixel was added to both ends of any sequence of three or more pixels. This was done to interdigitate any artifact gaps during the previous steps. The image was then skeletonized to reduce the signal down to a single-pixel thickness and then inverted from a light-on-dark background to a dark-on-light background. Inversion is required to visualize the gating process. The software generates regions around all of the signal objects in the image and then copies them into the original image, making length measurements within the respective established regions. Data are generated as measurement-output files for all individual regions. The sum of all regions constitutes the total neurite length for the entire image.

Statistical Analysis. Data were analyzed by two-way (group × time), repeated measures ANOVA. One-tailed, paired, Student's *t* tests were Bonferroni/Sidak corrected for the number of preplanned, nonorthogonal comparisons *post hoc*. Data were analyzed by ANOVA using the general linear models procedure of SAS (SAS Institute Inc., Cary, NC).

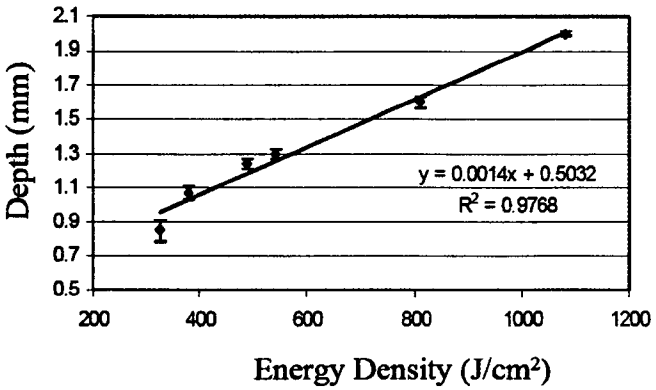

Figure 1. The relationship between energy density and depth of penetration. Laser settings used: power, 120 W; focal distance, 260 mm; beam delivery pattern, 100 mm^2; pulse duration, 0.45 secs; and seven pulses of varying energy density per pulse with a 2-sec interval between each pulse (linear correlation; $R^2 = 0.9768$; $n = 32$).

Results

We were interested in generating a reproducible, deep-dermal injury resulting in the removal of 100% of the epidermis and approximately 50% of the dermis. Shown in Figure 1 is wound depth as a function of increasing laser energy densities that indicates a linear relationship between energy density and depth of penetration ($R^2 = 0.9768$). Normal rat skin was determined to have a thickness of 2.05 ± 0.04 mm. The small variance observed in our measurements probably arises from prior barium-sulfide treatment establishing hair growth–cycle synchronization. Data indicate that wound depth correlates well with the amount of energy delivered by the laser. Energy densities above 1100 J/cm^2 resulted in complete tissue obliteration. It was determined that the laser energy needed to generate an injury exhibiting 50% dermal collagen depth was 378 J/cm^2 delivered in seven pulses of 54 J/cm^2 per pulse (Fig. 1). Using these laser settings, deep epithelial structures and subcutaneous adipose tissue remained unaffected (Fig. 2B) when compared to laser-untreated control (Fig. 2A) and are comparable to a partial, superficial-thickness burn. In contrast, energy densities above 486 J/cm^2 exhibited coagulative necrosis of surface epithelium and dermal connective tissue, blood vessels, and adnexa with all epithelial components of the dermis affected (data not shown). Thus, energy densities greater than 486 J/cm^2 generated 80%–90% tissue ablation and were comparable to a full-thickness burn. In all examined samples, histologic data showed a consistent-control (laser untreated) skin depth of 2.05 ± 0.04 mm and a viable skin depth of 0.95 ± 0.07 mm following laser ablation.

Gross and histologic evaluation of the laser-induced wound as a function of time is shown in Figure 2C (Day 0–Day 21). At Day 0 postinjury, wounds were characterized by coagulative necrosis of surface epithelium and partial dermal connective tissue, blood vessels, and adnexa, with deep epithelial components of the dermis unaffected. Necrosis did not extend beyond the deep dermis onto the panniculus layers of the hypodermis. Necrotic change in the dermis produced an accumulated mass of material that lacked organization or structure. Histologically, the dermal changes exhibited color with hematoxylin-eosin staining that varied from brightly eosinophilic (near the surface) to lightly eosinophilic to basophilic at the deepest margin. Light eosinophilic-to-basophilic color changes occurring at the deepest margin of the lesion were associated with degenerating collagen that maintained some structural integrity. Multifocally, there was neutrophilic inflammation present along the deep margins of the injury. The dermis immediately adjacent to the areas of necrosis and degeneration exhibited widely separated collagen fibers (i.e., edema) and congestion. The wound showed signs of healing as well as slight contraction by Day 7 postinjury. Scab formation was evident by Day 14, with re-epithelization of the wound underneath the scab. By Day 21 postinjury, the wound appeared healed at the gross level, but continued to exhibit histologic signs of healing compared to uninjured control. Axonal outgrowth assessment showed a clear decrease in stained axons at the injury site after laser ablation, and the number of neurites increased with time after injury. During the method-development phase, Day 14 was empirically determined to be optimal with regard to neurite outgrowth measurement. Animals were sacrificed and tissue was harvested at Days 0, 3, 7, 14, and 21 postinjury. All samples were stained for NF-200 reactivity (data not shown).

To establish that no bias mediated *via* infection or inflammation occurred, standard blood chemistries and complete blood counts were carried out using blood from animals subjected to laser ablation as described above. Complete blood counts were performed on Day 7 post–laser treatment. All parameters measured (i.e., white blood cell count, red blood cell count, hemoglobin, hematocrit, mean corpuscular volume, mean corpuscular hemoglobin, mean corpuscular hemoglobin concentration, platelet count, leukocyte subpopulation differential) were within the normal range (data not shown). Similarly, all blood chemistry parameters measured (i.e., alanine aminotransferase; albumin; alkaline phosphatase; aspartate aminotransferase; conjugated, unconjugated, and total bilirubin; calcium; carbon dioxide; cholesterol; creatinine; gamma glutamyl transferase; glucose; lactate dehydrogenase; magnesium; potassium; sodium; total protein; urea nitrogen; uric acid) were within normal range (data not shown). Additionally, pain/distress was monitored daily and all animals exhibited normal grooming, posture, appetite, and weight gain during the postinjury period (data not shown).

As shown in Figure 3A, saline-treated wounds exhibited considerable NK-1 receptor immunoreactivity, which increased significantly in the presence of exogenous SP. Pretreatment of the wound with the SP antagonist SII before the addition of SP administration significantly reduced the SP effect.

As shown in Figure 3B, SP exhibited a significant

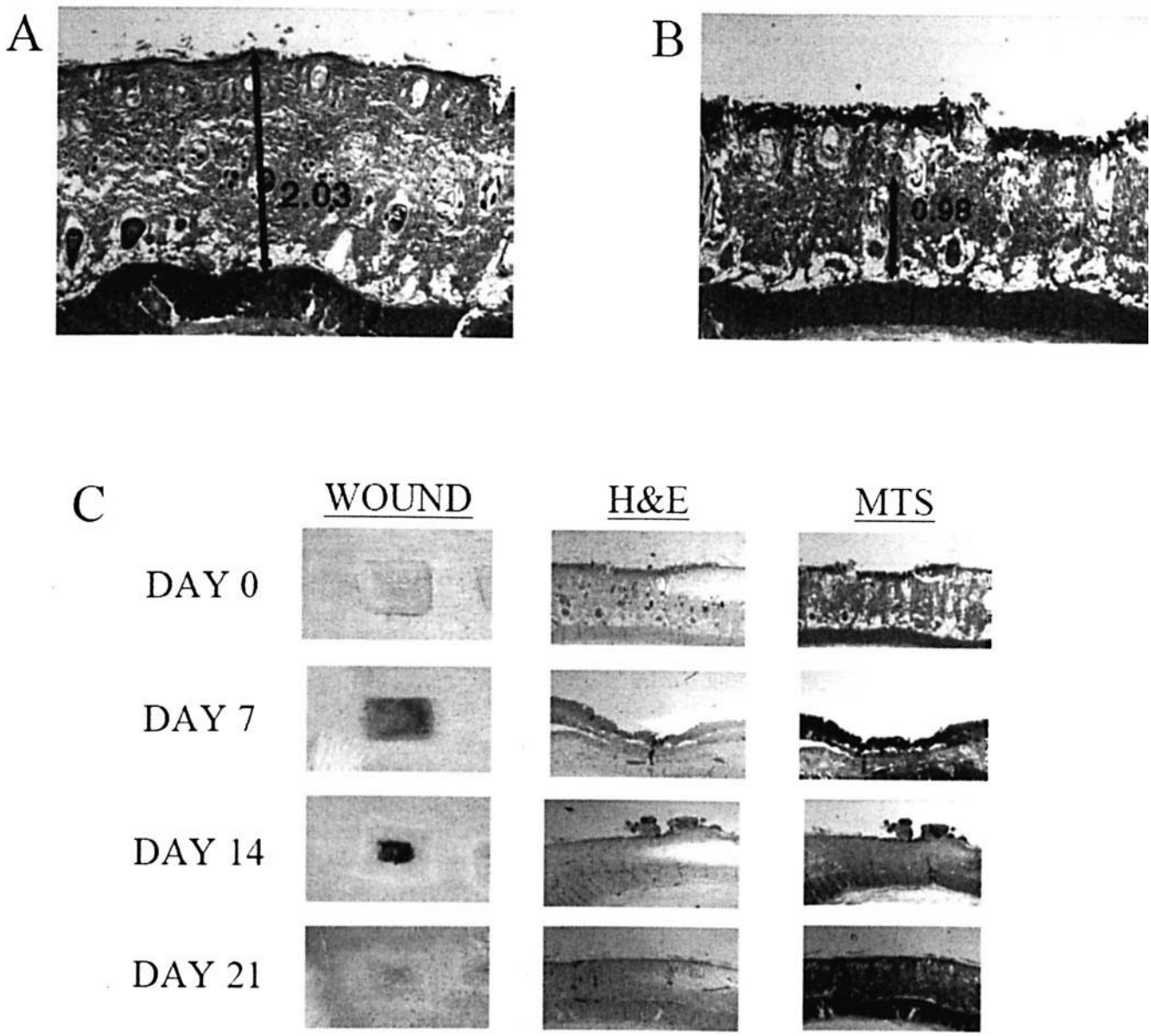

Figure 2. Representative images of histologically stained control and laser-induced, injured rat skin. (A) Normal rat skin. (B) Laser-induced injury (calibrated measurements are expressed in mm). (C) Representative images (gross wound appearance and routine histologic evaluation) of untreated wound-healing time course. H&E, hemotoxylin-eosin; MTS, Mason's Trichrome Stain.

effect upon neurite outgrowth. Fluorescence-intensity measurements indicated that an SP concentration of 10^{-10} *M* had little effect on neurite outgrowth compared to the saline control. In contrast, SP concentrations of 10^{-7} *M* and 10^{-4} *M* showed statistically significant differences in neurite outgrowth when compared to the saline control. In similar fashion as described for NK-1 receptor fluorescence, pretreatment of the injury with an SP antagonist reduced the effect of added SP. Using the "total-length" method for quantitating neurite outgrowth, results were much more definitive. As shown in Figure 3C, all tested SP concentrations showed statistically significant ($P < 0.05$) increases compared to the saline-treated control. Pretreatment with SII exhibited total inhibition of the SP treatment ($P < 0.05$).

As shown in Figure 4, gross examination of saline-treated wounds exhibited scab formation at the surface of the wound and covered approximately 80% of the total surface of the respective wound area (approximate mean size of 79.2 ± 8.4 mm^2). In contrast, visual examination of SP-treated wounds revealed markedly improved healing compared to untreated control. Both wound size and scab formation exhibited significant decreases as a function of increasing SP concentration. Consistent with previously noted effects of pretreatment of the wound with SII before SP treatment, wound surface area was observed to increase, postinjury, (Fig. 4).

Gross examination of the wound area revealed SP administration to significantly affect scab formation; how-

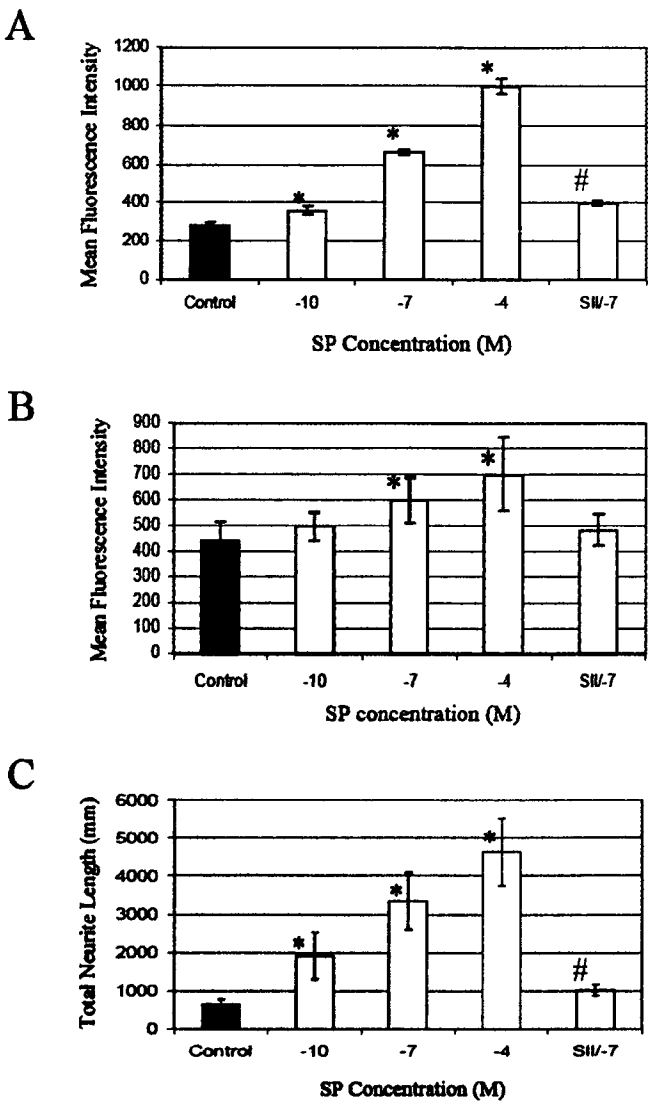

Figure 3. The effect of Substance P (SP) treatment on neurokinin-1 receptor length and total neurite length. All measurements were made as previously described in the Materials and Methods section. (A) Neurokinin-1 receptor total mean fluorescence-intensity measurements for saline- and Substance P–treated, laser-injured animals with various Substance P concentrations (*i.e.*, 10^{-10} *M*, 10^{-7} *M*, and 10^{-4} *M*) and 10^{-6} *M* Spantide II pretreatment followed by 10^{-7} *M* Substance P treatment on Day 0 postinjury. (B) Total mean fluorescence-intensity measurements. (C) Total neurite length measurements for saline-treated control. Closed bars, saline-treated controls; open bars, Substance P–treated animals; dashed bars, Spantide II pretreated plus Substance P 10^{-7} *M* treatment; *, value is significantly ($P < 0.05$) different from the saline-treated value; #, value is significantly ($P < 0.05$) different from the 10^{-7} *M* Substance P–treated value. Data represent means ± SE ($n = 10$).

ever, the most dramatic changes were observed histologically when compared to saline-treated control animals. Ranking (i.e., scoring 1–10) of these changes and their compilation is shown in Figure 5. The composite wound score for saline-treated control animals was approximately 9.5 ± 0.6 compared to 5.3 ± 1.0, 4.2 ± 0.8, and 4.0 ± 0.8 for 10^{-10} *M*, 10^{-7} *M*, and 10^{-4} *M* SP-treated wounds, respectively. Consistent with the effect of the SP antagonist

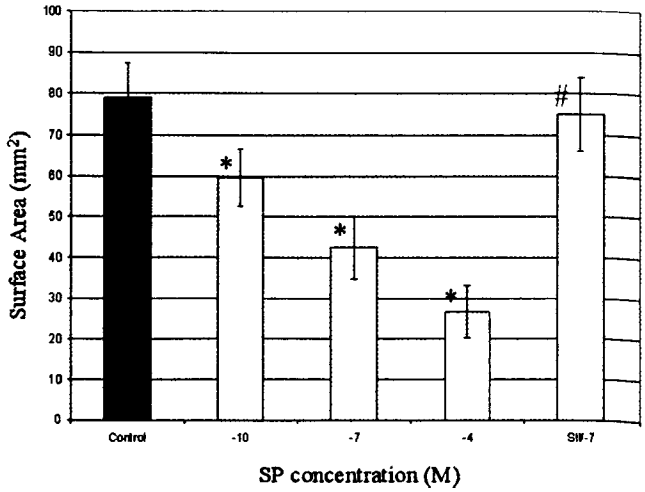

Figure 4. Total wound surface area as a function of Substance P (SP) treatment. Total wound surface area measurements for saline-treated control. Concentrations of Substance P used (*i.e.*, 10^{-10} *M*, 10^{-7} *M*, and 10^{-4} *M*) and 10^{-6} *M* Spantide II pretreatment followed by 10^{-7} *M* Substance P treatment on Day 0 postinjury. Closed bars, saline-treated controls; open bars, Substance P–treated animals; dashed bars, Spantide II pretreated plus Substance P 10^{-7} *M* treatment; *, value is significantly ($P < 0.05$) different from the saline-treated value; #, value is significantly ($P < 0.05$) different from the 10^{-7} *M* Substance P–treated value. Data represent means ± SE ($n = 10$).

SII, the composite wound-healing score was essentially increased to that observed for saline-treated controls (Fig. 5).

Shown in Figure 6 is the effect of exogenous SP on the expression of ICAM-1, indicating that the total percentage of leukocytes expressing ICAM-1 did not differ significantly from that observed for both saline- and SP-treated animals (Fig. 6A). However, SP treatment altered the number of ICAM-1 molecules expressed per cell ($P < 0.05$; Fig. 6B).

As shown in Figure 7A, the effect of SP on $\alpha_5\beta_1$-integrin molecule immunofluorescence was observed to be increased significantly for all SP concentrations compared to the saline control. Pretreatment of the wound with SII before SP treatment significantly decreased $\alpha_5\beta_1$-integrin molecule immunofluorescence.

Quantitation of leukocytes infiltrating the wound was determined and exhibited a similar pattern to that observed for ICAM-1. This infiltration phenomenon is a direct effect of the $\alpha_5\beta_1$ integrin-adhesion molecule. As shown in Figure 7B, 10^{-7} *M* and 10^{-4} *M* SP increased leukocyte infiltration significantly when compared to the saline-treated controls. Pretreatment of the wound with SII before SP treatment reversed the infiltration of leukocytes essentially to that observed for saline-treated controls.

Discussion

The purposes of this study were to develop a novel animal skin–injury model that would be suitable for studying wound healing and to investigate the effect of

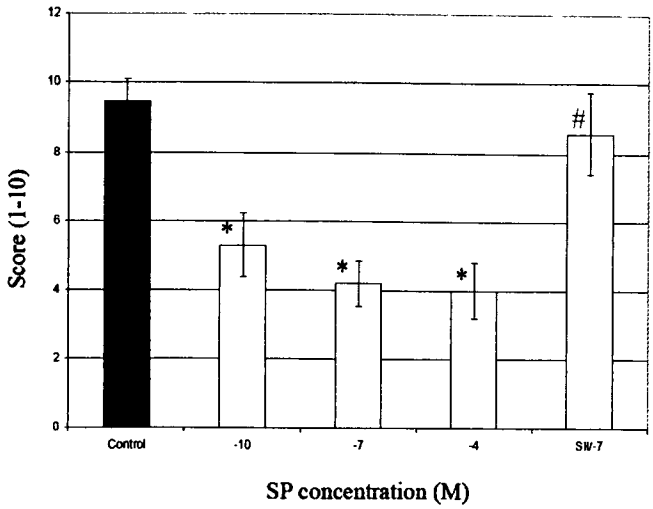

Figure 5. Wound-healing scores as a function of Substance P treatment. Wound-healing scoring was performed as previously described in the Materials and Methods section. Concentrations of Substance P (SP) used (*i.e.*, 10^{-10} *M*, 10^{-7} *M*, and 10^{-4} *M*) and 10^{-6} *M* Spantide II pretreatment followed by 10^{-7} *M* Substance P treatment on Day 0 postinjury. Closed bars, saline-treated controls; open bars, Substance P–treated animals; dashed bars, Spantide II pretreated plus Substance P 10^{-7} *M* treatment; *, value is significantly ($P < 0.05$) different from the saline-treated value; #, value is significantly ($P < 0.05$) different from the 10^{-7} *M* Substance P–treated value. Data represent means ± SE ($n = 10$).

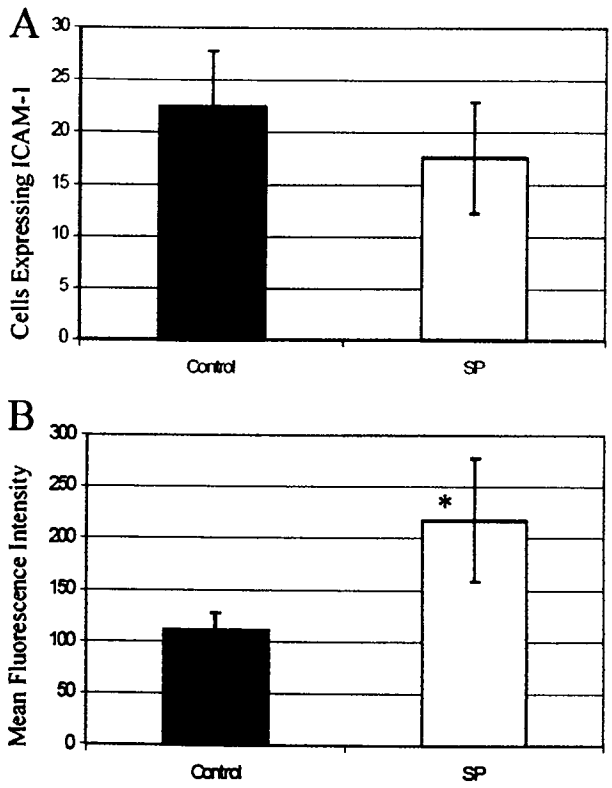

Figure 6. The effect of Substance P (SP) treatment on expression of intercellular adhesion molecule-1. Detection of intercellular adhesion molecule-1 was performed as described in the Materials and Methods section. (A) Percentage of cells expressing intercellular adhesion molecule-1 in response to treatment with saline (closed bars) and 10^{-7} *M* Substance P (open bars) on Day 0 postinjury. (B) Mean fluorescence intensity per cell in response to treatment with saline (closed bars) and 10^{-7} *M* Substance P (open bars). *, value is significantly ($P < 0.05$) different from the saline-control value. Data represent means ± SE ($n = 6$).

exogenously added SP on the healing of a CO_2 laser–induced injury. Thus, the first major issue addressed in this study was the utility of the CO_2 laser in generation of precise and reproducible deep-dermal injury. Gross and histologic examination of the effects of a CO_2 laser of varying energy densities on epilated rat skin were investigated and indicated no evidence of charring, lesions were nonhemorrhagic, and margins were clearly defined for all tested energy densities. Energy densities greater than 1100 J/cm^2 resulted in total ablation of all epidermal and dermal layers. Furthermore, our energy-density findings are consistent with studies using the CO_2 laser for tissue debridement associated with cutaneous resurfacing surgery (25–27). Although not shown, laser dwell time significantly affected wound reproducibility. Thus, a dwell time of 49 milliseconds was essential for generating highly reproducible wound-depth measurements and reducing thermal damage zones within the wound's edges. This finding is corroborated by a similar observation by Domankevitz and Nishioka (28) using a porcine skin model.

This investigation has established that the energy density used generates consistent laser-ablation wound depths of 0.95 ± 0.07 mm. Likewise, hair follicle synchronization gives rise to consistent control skin depths of 2.05 ± 0.04 mm. This is the first study to present data that exhibit such low variance for rat skin, which is of extreme importance with regard to the number of animals required for statistical significance (reduced substantially). This novel-injury model represents a new platform for the study of wound healing.

The second major issue addressed in this study was determining the effect of exogenously added SP on the initiation of tissue repair in well-defined, laser-induced, injured tissue. It is well established that SP is synthesized and released by neurons (29, 30). A report by Menkes *et al.* (31) indicates elevated SP levels in synovium and synovial fluid from patients with rheumatoid arthritis and osteoarthritis. Navarro *et al.* (32) show that SP immunoreactivity was significantly increased after a mouse sciatic nerve–crush injury. In human burn wounds, Altun *et al.* (33) observe the presence of SP and nerve outgrowth during the remodeling phase. However, Gibran *et al.* (34) describe the reverse to be true in patients with diabetes mellitus who had impaired cutaneous healing indicating diminishing SP levels. They also observed an association between healing impairment and SP and concluded that the absence of SP directly contributes to the abnormal healing response in patients with diabetes (34).

It has been proposed that wound healing can be accelerated by exogenous administration of sensory peptides (35). Using a severe inflammation model, Bowles *et al.* (36) demonstrated that tissue levels of SP are increased (>8-

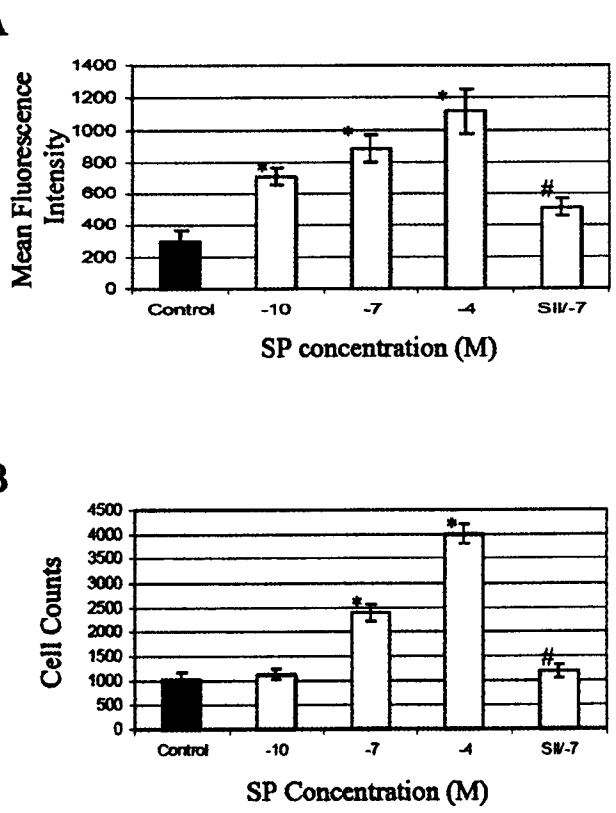

Figure 7. Effects of Substance P (SP) treatment on $\alpha_5\beta_1$-integrin molecule immunofluorescence and leukocyte infiltration. (A) $\alpha_5\beta_1$-integrin molecule immunofluorescence. Mean fluorescence intensity of saline-treated control and Substance P–treated animals with various Substance P concentrations (*i.e.*, 10^{-10} *M*, 10^{-7} *M*, and 10^{-4} *M*) and 10^{-6} *M* Spantide II pretreatment followed by 10^{-7} *M* Substance P treatment on Day 0 postinjury. (B) Infiltrating leukocyte counts. Total cell counts of saline-treated control and Substance P–treated injury animals with various Substance P concentrations (*i.e.*, 10^{-10} *M*, 10^{-7} *M*, and 10^{-4} *M*) and 10^{-6} *M* Spantide II pretreatment followed by 10^{-7} *M* Substance P treatment. Closed bars, saline-treated controls; open bars, Substance P–treated animals; dashed bars, Spantide II pretreated plus Substance P 10^{-7} *M* treatment; *, value is significantly ($P < 0.05$) different from the saline-treated value; #, value is significantly ($P < 0.05$) different from the 10^{-7} *M* Substance P–treated value. Data represent means ± SE ($n = 10$).

fold) in patients with irreversible pulpitis compared to normal dental pulp. Likewise, in a rat colon denervation model, the addition of the SP-enhanced neuronal area and the epithelial cell proliferation compared to saline-treated controls (37). Collectively, these studies suggest that SP has a primary role in tissue repair.

Although Bowden *et al.* (38) report NK-1 receptors to be internalized on SP binding, (39) there are published studies suggesting NK-1 receptors to be upregulated on activation (39–41). Data presented here that indicate increased NK-1 receptor immunoreactivity after the exogenous addition of SP are consistent with the conclusions of Velazquez *et al.* (40), who suggest an SP-mediated upregulation in rat spinal cord. However, it is possible that activation of the receptor may trigger either response depending on the cell type expressing the receptor or localized conditions *in situ* that may affect pathways that, in finality, affect the binding of ligand to receptor. Considering the most recent reports in nervous tissue, upregulation of the NK-1 receptor tends to be in vogue. An alternative possibility is that of new NK-1 receptor–bearing cells entering the wound area and giving rise to increased immunofluorescence. This possibility has been pursued by Weinstock *et al.* (42), who demonstrate the T-cell NK-1 receptor to be inducible following exposure to cytokines. Data presented here demonstrate a dose-dependent effect of SP on neurite outgrowth, which suggests a direct effect of SP or an SP metabolite on the regenerating axon consistent with the findings of Lindner *et al.* (43) and/or SP activation of cells at the site of injury, producing cytokines that in turn elicit secretion of neurotrophic factors (44–46).

In order for leukocytes to be activated by SP and produce cytokines required for tissue-repair signaling, they must first leave the vasculature and migrate into the site of injury, a process shown to occur *via* adhesion molecules. Data presented here indicate an SP dose–dependent infiltration of large numbers of leukocytes that is consistent with the observations of other investigators (47). Thus, if leukocytes are present at the site of injury, the cell surface molecules (*e.g.*, ICAM-1) mediating their migration should also increase as well. Our findings are consistent with the theme of upregulation of ICAM-1, (*i.e.*, the number of cells expressing ICAM-1 does not change, but the number of receptors per cell increases). Consistent with this theme, neutrophil accumulation in inflamed skin has been shown to be SP-receptor dependent (48).

It has been reported that both integrins and the extracellular matrix influence Schwann cell–axon interaction and myelination during the nerve-repair process (49). The effect of SP on integrin $\alpha_5\beta_1$, which mediates the binding of cells to fibronectin in the extracellular matrix, was investigated and observed to be significantly (~2.5-fold) increased following treatment with 10^{-10} *M* SP. Interestingly, synthesis of fibronectin and collagen has been shown increased at the site of injury, with higher concentrations in the region connecting the proximal and distal nerve endings playing a role in nerve repair (50). Furthermore, activation of the integrin gene dramatically improves regeneration of adult neurons (51), which suggests that SP could exert its effects *via* integrin-gene activation.

The interaction between peripheral nerves and the immune system occurs *via* cutaneous nerve fiber neuromediator release and their respective interaction(s) with receptors on specific target cells that potentially affects a variety of physiologic functions. Understanding the mechanisms involved in these processes should lead to identification of new and better therapeutic regimes for the treatment of cutaneous injury.

1. Payan DG, Goetzl EJ. Modulation of lymphocyte function by sensory neuropeptides. J Immunol 135(Suppl 2):783–786, 1985.
2. Li Y, Tian S, Douglas SD, Ho WZ. Morphine up-regulates expression

of substance P and its receptor in human blood mononuclear phagocytes and lymphocytes. Cell Immunol 205:120–127, 2000.
3. Lai XN, Wang ZG, Zhu JM, Wang LL. Effect of substance P in gene expression of transforming growth factor beta-1 and its receptors in rat's fibroblasts. Chin J Traumatol 6:350–354, 2003.
4. Smith PG, Liu M. Impaired cutaneous wound healing after sensory denervation in developing rats: effects on cell proliferation and apoptosis. Cell Tissue Res 307:281–291 2002.
5. Ho WZ, Lai JP, Li Y, Douglas SD. HIV enhances substance P expression in human immune cells. FASEB J 16:616–618, 2002.
6. Jansco N, Jansco-Gabor A, Szolcsanyi J. Direct evidence for neurogenic inflammation and its prevention by denervation and by pretreatment with capsaicin. Br J Pharmacol 31:131–151, 1967.
7. Ralevic V, Milner P, Hudlicka O, Kristek F, Burnstock G. Substance P is released from the endothelium of normal and capsaicin treated rat hind-limb vasculature in vivo, by increased flow. Circ Res 66:1178–1183, 1990.
8. Wallengren J, Hakanson R. Effects of substance P, neurokinin A and calcitonin gene-related peptide in human skin and their involvement in sensory nerve-mediated responses. Eur J Pharmacol 143:267–273, 1987.
9. Barnes PJ, Brown MJ, Dollery CT, Fuller RW, Heavey DJ, Ind PW. Histamine is released from skin by substance P but does not act as the final vasodilator in the axon reflex. Br J Pharmacol 88:741–745, 1986.
10. Holzer P. Local effector functions of capsaicin-sensitive sensory nerve endings: involvement of tachykinins, calcitonin gene-related peptide and other neuropeptides. Neuroscience 24:739–768, 1988.
11. Dunnick CA, Gibran NS, Heimbach DM. Substance P has a role in neurogenic mediation of human burn wound healing. J Burn Care Rehabil 17:390–396, 1996.
12. Bockers M, Benes P, Bork K. Persistent skin ulcers, mutilations and acro-osteolysis in hereditary sensory and autonomic neuropathy with phospholipid excretion. J Am Acad Dermatol 21:736–739, 1989.
13. Hagen NA, Stevens JC, Michet CJ. Trigeminal sensory neuropathy associated with connective tissue disease. Neurology 40:891–896, 1990.
14. Ziche M, Morbidelli L, Pacini M, Geppetti P, Alessandri G, Maggi CA. Substance P stimulates neovascularization in vivo and proliferation of cultured endothelial cells. Microvasc Res 40:264–278, 1990.
15. Namuri S, Fujita T. Stimulatory effects of substance P and nerve growth factor (NGF) on neurite outgrowth in embryonic chick dorsal root ganglia. Neuropharmacology 17:73–76, 1978.
16. Fan TP, Hu DE, Smither RL, Gresham GA. Further studies on angiogenesis in a rat sponge model. EXS 61:308–314, 1992.
17. Fan TP, Hu DE, Guard S, Gresham GA, Watling KJ. Stimulation of angiogenesis by substance P and interleukin-1 in the rat and its inhibition by NK1 or interleukin-1 receptor antagonists. Br J Pharmacol 110:43–49, 1993.
18. Nilsson J, von Euler AM, Dalsgaard CJ. Stimulation of connective tissue cell growth by substance P and substance K. Nature 315:63–63, 1985.
19. Kahler CM, Reinisch N, Wiederman CJ. Interaction of SP with epidermal growth factor and fibroblast growth factor in cyclooxygenase-dependent proliferation of human skin fibroblasts. J Cell Physiol 166:601–608, 1996.
20. McGovern UB, Jones KT, Sharpe GR. Intracellular calcium as a second messenger following growth stimulation of human keratinocytes. Br J Dermatol 132:892–896, 1995.
21. Tanaka TT, Danno K, Ikai K, Imamura S. Effects of substance P and substance K on the growth of cultured keratinocytes. J Invest Dermatol 90:399–401, 1988.
22. Wollina U. The effect of neuropeptides on wound healing in vitro and in vivo. Hautarzt 43:616–620, 1992.
23. Zawacki BE, Jones RJ. Standard depth burns in the rat: the importance of the hair growth cycle. Br J Plast Surg 20:347–354, 1967.
24. McCarthy BG, Hsieh ST, Stocks A, Hauer P, Macko C, Cornblath DR, Griffin JW, McArthur JC. Cutaneous innervation in sensory neuropathies: evaluation by skin biopsy. Neurology 41:1848–1855, 1995.
25. Weisberg NK, Kuo T, Torkian B, Reinisch L, Ellis DL. Optimizing fluence and debridement effects on cutaneous resurfacing carbon dioxide laser surgery. Arch Dermatol 134:1223–1228, 1998.
26. Collawn SS. Re-epithelialization of the skin following CO_2 laser resurfacing. J Cosmet Laser Ther 3:123–127, 2001.
27. Mison MB, Steficek B, Lavagnino M, Teunissen BD, Hauptman JG, Walshaw R. Comparison of the effects of the CO_2 surgical laser and conventional surgical techniques on healing and wound tensile strength of skin flaps in the dog. Vet Surg 32:153–160, 2003.
28. Domankevitz Y, Nishioka NS. Effects of a rapid scanned carbon dioxide laser on porcine dermis. J Burn Care Rehabil 18:206–209, 1997.
29. Pernow B. Substance P. Pharmacol Rev 35:85–141, 1983.
30. White DM. Release of substance P from peripheral sensory nerve terminals. J Peripher Nerv Syst 2:191–201, 1997.
31. Menkes CJ, Renoux M, Laoussadi S, Mauborgne J, Cesselin F. Substance P levels in the synovium and synovial fluid from patients with rheumatoid arthritis and osteoarthritis. J Rheumatol 20:714–717, 1993.
32. Navarro X, Verdu E, Wendelschafer-Crabb G, Kennedy WR. Immunohistochemical study of skin reinnervation by regenerative axons. J Comp Neurol 380:164–174, 1997.
33. Altun V, Hakvoort TE, van Zuijlen PP, van der Kwast TH, Prens EP. Nerve outgrowth and neuropeptide expression during the remodeling of human burn wound scars: a 7-month follow-up study of 22 patients. Burns 27:717–722, 2001.
34. Gibran NS, Jang YC, Isik FF, Greenhalgh DG, Muffley LA, Underwood RA, Usui ML, Larsen J, Smith DG, Bunnett N, Ansel JC, Olerud JE. Diminished neuropeptide levels contribute to the impaired cutaneous healing response associated with diabetes mellitus. J Surg Res 108:122–128, 2002.
35. Khalil Z, Helme R. Sensory peptides as neuromodulators of wound healing in aged rats. J Gerontol A Biol Sci Med Sci 51:B354–B361, 1996.
36. Bowles WR, Withrow JC, Lepinski AM, Hargreaves KM. Tissue levels of immunoreactive substance P are increased in patients with irreversible pulpitis. J Endod 29:265–267, 2003.
37. Buttow NC, Zucoloto S, Espreafico EM, Gama P, Alvares EP. Substance P enhances neuronal area and epithelial cell proliferation after colon denervation in rats. Dig Dis Sci 48:2069–2076, 2003.
38. Bowden JJ, Garland AM, Baluk P, Lefevre P, Grady EF, Vigna SR, Bunnett NW, McDonald DM. Direct observation of substance P-induced internalization of neurokinin 1 (NK1) receptors at sites of inflammation. Proc Natl Acad Sci U S A 91:8964–8968, 1994.
39. King KA, Hu C, Rodriguez MM, Romaguera R, Jiang X, Piedimonte G. Exaggerated neurogenic inflammation and substance P receptor regulation in RSV-infected weanling rats. Am J Respir Cell Mol Biol 24:101–107, 2001.
40. Velazquez RA, McCarson KE, Cai Y, Kovacs KJ, Shi Q, Evensjo M, Larson AA. Upregulation of neurokinin-1 receptor expression in rat cord by an N-terminal metabolite of substance P. Eur J Neurosci 16:229–241, 2002.
41. Shi X, Gao NR, Guo QM, Yang YJ, Huo MD, Hu HL, Friess H. Relationship between overexpression of NK-1R, NK-2R and intestinal mucosal damage in acute necrotizing pancreatitis. World J Gastroenterol 9:160–164, 2003.
42. Weinstock JV, Blum A, Metwali A, Elliot D, Arsenescu R. IL-18 and IL-12 signal through the NK-kappa B pathway to induce NK-1R expression on T cells. J Immunol 170:5003–5007, 2003.
43. Lindner G, Grosse G, Jentzch KD, Oehme P, Wenzel M. Effect of

derivatives of substance P dipeptide on nerve fiber growth in tissue culture. J Hirnforsch 27:639–649, 1986.

44. Narumi S, Fujita T. Stimulatory effects of substance P and nerve growth factor (NGF) on neurite outgrowth in embryonic chick dorsal root ganglia. Neuropharmacology 17:73–76, 1978.
45. Farhadieh RD, Nicklin S, Yu Y, Gianoutosos MP, Walsh WR. The role of nerve growth factor and brain-derived neurotrophic factor in inferior alveolar nerve regeneration in distraction osteogenesis. J Craniofac Surg 14:859–865, 2003.
46. Lee AC, Yu VM, Lowe JB, Brenner MJ, Hunter DA, Mackinnon SE, Sakiyama-Elbert SE. Controlled release of nerve growth factor enhances sciatic nerve regeneration. Exp Neurol 184:295–303, 2003.
47. Kahler CM, Pischel A, Kaufman G, Wiedermann CJ. Influence of neuropeptides on neutrophil adhesion and transmigration through a lung fibroblast barrier in vitro. Exp Lung Res 27:25–46, 2001.
48. Cao T, Grant AD, Gerard NP, Brain SD. Lack of significant effect of deletion of the tachykinin neurokinin-1 receptor on wound healing in mouse skin. Neuroscience 108:695–700, 2001.
49. Kuhn T, Schmidt M, Kater S. Laminin and fibronectin guidepost signal sustained but opposite effects to passing growth cones. Neuron 14:275–285, 1995.
50. Lefcort F, Venstrom K, McDonald JA, Reichardt LF. Regulation of the expression of fibronectin and its receptor $\alpha 5\beta 1$, during developing and regeneration of peripheral nerve. Development 116:767–782, 1992.
51. Condic ML. Adult neuronal regeneration induced by transgenic integrin expression. J Neurosci 21:4782–4788, 2001.